Jiang, Q., et al., 2020, Longest continuously erupting large igneous province driven by plume-ridge interaction: Geology, v. 49, https://doi.org/10.1130/G47850.1

Supplementary Material

Outline of supplemental material

I. Compilation of previous age data and criteria for reliable age

II. Recalculation of previous ages using the ^{40}K decay constants revised by Renne et al. (2011)

III. Sample acquisition, description and analytical methods

IV. $^{40}Ar/^{39}Ar$ analytical results

V. Mantle source components of the Kerguelen large igneous province in Figure 4

VI. Formation of the Ninetyeast Ridge and Northern Kerguelen Plateau

- Figures S1–8
- Tables S1–3

Supplementary data in separate files

- Table S4. Full $^{40}Ar/^{39}Ar$ data for new analyses from the Kerguelen large igneous province
- Table S5. Compilation of Sr–Nd–Pb isotopic analyses from the Kerguelen large igneous province

I. Compilation of previous age and criteria for reliable age

Compiled $^{40}Ar/^{39}Ar$ age data of basalts from the Cretaceous Central and Southern Kerguelen Plateau, Elan Bank and Broken Ridge are listed in Table S1. Our criteria for reliable ages are stated in Section III. A rigorous filtering of the compiled data resulted in four statistically reliable plagioclase $^{40}Ar/^{39}Ar$ ages for the main portion of the Greater Kerguelen large igneous province (LIP; Table S1).

II. Recalculation of previous ages using the ^{40}K decay constants revised by Renne et al. (2011)

$^{40}Ar/^{39}Ar$ age data reported by Duncan (2002) and Coffin et al. (2002) used ^{40}K decay constants of Steiger and Jäger (1977), which has been updated and calibrated against U-Pb data by Renne et al. (2010) and Renne et al. (2011). Therefore, these age data have been recalculated to the new ^{40}K constants and standards to allow direct comparison, and the results are presented in Table S2.

III. Sample acquisition, description and analytical methods

The ODP drill core basaltic samples were requested from the Kochi Core Center (Japan). Samples are only available from the topmost tens of meters of the basaltic layer penetrated by the ODP drill holes (Fig. S1), while a large portion of the basaltic layer has not been penetrated and is unavailable for sampling. Dredged samples of the *Marion Dufresne* cruise 48 (KG 83, 84, 87), *Robert Conrad* cruises 17 and 27 (KG 38, 40, 48, 50, 51), and USNS *Eltanin* Marine Geology cruise 46 (KG 43) were requested from the National Museum of Natural History (France), Polar Rock Repository (USA) and Lamont-Doherty Core Repository (USA), respectively.

The samples are typically dark grey, sparsely vesicular, porphyritic rocks with fine-grained groundmass. Most of the samples are basalt. Some samples from Site 1137 on Elan Bank are

slightly evolved basalt and basaltic andesite. Thin sections show that the samples contain 2% (e.g., KG16, KG48) to 30% (KG32) plagioclase (or sanidine) up to 6 mm long. Two samples (KG25, KG26) from Site 748 are likely to be either trachybasalt or basaltic trachy-andesite according to the major element compositions of samples from the same drill core interval (Shipboard Scientific Party, 1989) and contain sanidine (cf. EDX analyses in Fig. S2). Some samples contains 2% to 10% augite from 0.1 to 2 mm in length.

Samples were first crushed with a clean tungsten carbide hydraulic press and mill, and then sieved to size fractions of 212–355 μm and 125–212 μm. The sample fractions were thoroughly rinsed with distilled water in an ultrasonic cleaner to remove any dust or powder from the desired grains. Minerals were separated using a Frantz isodynamic magnetic separator. Plagioclase, sanidine, pyroxene and glass grains that were unaltered, optically transparent and free from inclusions were carefully handpicked grain-by-grain under a binocular microscope from either the 125–212 μm or the 212–355 μm size, non-magnetic (plagioclase and sanidine) or low magnetic (pyroxene and glass) fractions. Homogenous groundmass grains were handpicked from the magnetic fractions. However, even though potential signs of alteration (e.g., brown, red or yellow discolouration) were avoided where possible, cryptic alteration cannot be easily observed since groundmass is not transparent. The selected mineral and groundmass grains were leached in diluted (5 N) HF for one minute and then thoroughly rinsed in distilled water.

Multi-grain aliquots of the samples were loaded into several large wells of 1.9 cm diameter and 0.3 cm depth aluminium discs. A series of fully intercalibrated FC sanidine (Jourdan and Renne, 2007) and GA1550 biotite (Renne et al., 1998) standards, for which ages of 28.294 ± 0.037 Ma and 99.738 ± 0.100 Ma (Renne et al., 2011) were used, were loaded alongside with the samples in the same discs (Fig. S3) and were irradiated for 40 hours. The discs were Cd-shielded to

minimize undesirable nuclear interference reactions and irradiated in the Oregon State University nuclear reactor (USA) in central position. For each disc, an average J-value was computed from standard grains within the small pits, and was used in the age calculations of samples in the surrounding pits of the disc. The J-value for each sample is shown in Table S4. Mass discrimination was monitored regularly through the analysis using an automated air pipette and provided mean values of 0.99368 ± 0.17, 0.9935 ± 0.07, 0.99199 ± 0.24, 0.99093 ± 0.03, 0.99035 ± 0.03, 0.989721 ± 0.02, 0.989686 ± 0.03, 0.988646 ± 0.04, 0.987835 ± 0.07, 0.98782 ± 0.05 and 0.987368 ± 0.03 (%1σ) per dalton (atomic mass unit) relative to an air ratio of 298.56 ± 0.31 (2σ; Lee et al., 2006). The correction factors for interfering isotopes were $(^{39}Ar/^{37}Ar)_{Ca}$ = 6.95 × 10^{-4} (± 1.3%), $(^{36}Ar/^{37}Ar)_{Ca}$ = 2.65 × 10^{-4} (± 0.84%) and $(^{40}Ar/^{39}Ar)_{K}$ = 7.30 × 10^{-4} (± 12%; Renne et al., 2013), from which the most important correction value needed for Ca-rich samples like plagioclase and pyroxene was re-measured internally in 2017 and yielded a value of $(^{36}Ar/^{37}Ar)_{Ca}$ = 2.65 × 10^{-4} (± 1.6%), in agreement with the value measured by Renne et al. (2013). The $^{40}Ar/^{39}Ar$ analyses were performed at the Western Australian Argon Isotope Facility at Curtin University. Multi-grain aliquots of mineral crystals and groundmass were step-heated using a continuous 100 W PhotonMachine© CO_2 (IR, 10.4 μm) laser fired on the crystals for 60 s. Each of the standard crystals was fused in a single step.

The gas was purified in an extra low-volume stainless steel extraction line of 240cc and using one SAES AP10 and one GP50 getter. Ar isotopes were measured in static mode using a low volume (600 cc) ARGUS VI mass spectrometer from Thermofisher© (Phillips and Matchan, 2013) set with a permanent resolution of ~200. Measurements were carried out in multi-collection mode using four faradays to measure mass 40 to 37 and an ultra-low background compact discrete dynode ion counter to measure mass 36. We measured the relative abundance

of each mass simultaneously using 10 cycles of peak-hopping and 16 s of integration time for each mass. Detectors were calibrated to each other electronically and using air shot beam signals. The raw data were processed using the ArArCALC software (Koppers, 2002) and the ages have been calculated using the decay constants recommended by Renne et al. (2011). Blanks were monitored every 3 to 4 steps. All parameters and relative abundance values are provided in Table S4 following recommendations of Schaen et al. (2020) and have been corrected for blank, mass discrimination and radioactive decay.

Our criteria for the determination of plateau are as follows:

(1) $^{40}Ar/^{39}Ar$ plateaus obtained from fresh mineral separates are preferred than from groundmass.

(2) $^{40}Ar/^{39}Ar$ plateaus must include at least 70% of the released ^{39}Ar (Baksi, 2007; Ware and Jourdan, 2018). We use mineral mini-plateau (with 50–70% ^{39}Ar released) ages only if they are corroborated by a mineral separate plateau age from the sample or formation. Similarly, groundmass plateau (with >70% ^{39}Ar released) must be corroborated by one or more plateau ages on mineral separates. This is because groundmass samples are prone to be affected by ^{39}Ar recoil loss (Jourdan et al., 2007; Renne et al., 2015) and/or potassium leaching due to hydrothermal alteration that can lead to older apparent plateau ages (cf. plagioclase vs. groundmass plateau ages in Fig. S5A), and ^{40}Ar loss and/or recrystallization from cryptic hydrothermal alteration, which is much harder to visually detect than in mineral separates (Hofmann et al., 2000), especially for submarine basalts and will lead to younger apparent plateau ages (cf. Fig. S5B, Merle et al., 2019).

(3) The plateaus should be defined by at least 3 consecutive steps agreeing at 95% confidence level and satisfying a probability of fit (p) of at least 0.05. (4) $^{40}Ar/^{36}Ar$ intercepts need ideally to

overlap with the atmospheric $^{40}Ar/^{36}Ar$ ratio of 298.56 ± 0.31 (Lee et al., 2006). If the $^{40}Ar/^{36}Ar$ composition of the trapped argon measured using statistically reliable $^{39}Ar/^{40}Ar–^{36}Ar/^{40}Ar$ isochron (p > 0.05) differs from an atmospheric value, then the measured ratio and its uncertainties are used in the age spectrum model age calculation, following the approach of Oostingh et al. (2017).

Plateau ages are given at the 2σ level and are calculated using the mean of all the plateau steps, each weighted by the inverse variance of their individual analytical error. Uncertainties include analytical and J-value errors. Preferred plateau ages with all sources of uncertainties calculated following the error propagation approach of Renne et al. (2010) based on Monte Carlo simulations and appropriate R-values are provided in Table S3.

IV. $^{40}Ar/^{39}Ar$ analytical results

The analytical results are summarised in Table S3. $^{40}Ar/^{39}Ar$ apparent age versus cumulative ^{39}Ar released are shown in Fig. 2, Figs. S4–6.

Site 738, Southern Kerguelen Plateau

Two plagioclase and three groundmass samples were analyzed. The plagioclase plateau age of 113.0 ± 3.5 Ma (MSWD = 1.06; p = 0.38; KG6) and mini-plateau age of 109.5 ± 1.4 Ma (MSWD = 1.97; p = 0.06; ^{39}Ar = 50%; KG10) overlap with each other. One groundmass sample yielded a plateau age of 126.7 ± 1.5 Ma (MSWD = 1.35; p = 0.22; KG9), which is significantly older than the plagioclase ages and might be caused by K leaching due to alteration. Such a case nicely illustrates why groundmass results can be deceptive and must be treated with caution. The other two groundmass samples (KG8 and KG10) failed to yield plateau ages. The plagioclase plateau age of 113.0 ± 3.5 Ma is considered as the age of basalts from this site.

Site 748, Southern Kerguelen Plateau

Two sanidine aliquots from two samples were analyzed and they yielded $^{40}Ar/^{39}Ar$ plateau ages of 96.49 ± 0.35 Ma (MSWD = 0.45; p = 0.96; KG25) and 96.79 ± 0.42 Ma (MSWD = 0.38; p = 0.99; KG26), which overlap with each other at 2σ.

Site 749, Southern Kerguelen Plateau

Two plagioclase samples were analyzed. The $^{40}Ar/^{36}Ar$ intercept of 282.3 ± 6.2 (2σ) does not overlap with the atmospheric $^{40}Ar/^{36}Ar$ ratio of 298.56 ± 0.31 (2σ; Lee et al., 2006), so the measured intercept ratio was used to calculate a plateau age of 122.2 ± 2.0 Ma (MSWD = 0.28; p = 1; KG32), which is by definition in agreement with the isochron age of 122.2 ± 2.6 Ma (MSWD = 0.31; p = 1.00). The other sample (KG28) failed to yield a plateau.

Site 750, Southern Kerguelen Plateau

Two groundmass and one pyroxene samples were analyzed. The groundmass samples yielded plateau ages of 120.5 ± 3.3 Ma (MSWD = 0.35; p = 0.99; KG52) and 118.1 ± 3.5 Ma (MSWD = 0.38; p = 0.99; KG54). Both groundmass samples are older than previously reported $^{40}Ar/^{39}Ar$ plateau age of 113.45 ± 0.83 Ma (Coffin et al., 2002) obtained on plagioclase and might be secondary effects such as K loss due to alteration. The pyroxene sample yielded a plateau age of 117 ± 10 Ma (MSWD = 1.08; p = 0.36; KG53), and its large uncertainty inhibits its usefulness in constraining an eruptive age. Therefore, the previously acquired plagioclase age of 113.45 ± 0.83 Ma (Coffin et al., 2002) is the best age for recording crystallization of basalts from this site.

Site 1136, Southern Kerguelen Plateau

One analyzed plagioclase sample (KG57) did not yield a plateau age and therefore, previously published ages of 121.0 ± 2.1 Ma and 120.8 ± 2.1 Ma (Duncan, 2002) are the most robust ages for Site 1136.

MD 48-40, Southern Kerguelen Plateau

Four dredged samples were dated from this site, including three plagioclase separates, three pyroxene separates and one groundmass separate. Two plagioclase samples yielded $^{40}Ar/^{39}Ar$ plateau ages of 89.93 ± 0.97 Ma (MSWD = 1.32; p = 0.20; KG83R) and 95.28 ± 0.44 Ma (MSWD = 0.98; p = 0.44; KG84). These ages are interpreted as late stage volcanic activity on the Southern Kerguelen Plateau. The other plagioclase (KG83), pyroxene (KG83, KG84, KG87) and groundmass (KG100) samples did not yield plateaus.

Site 1137, Elan Bank

Six plagioclase and one pyroxene separates were analyzed from six samples (Fig. S6, Table S3). The plagioclase samples yielded plateau ages of 110.32 ± 0.34 Ma (MSWD = 1; p = 0.46; KG62), 113.3 ± 1.1 Ma (MSWD = 1.64; p = 0.06; KG63), 110.01 ± 0.43 Ma (MSWD = 1.41; p = 0.10; KG65), 106.09 ± 0.99 Ma (MSWD = 0.67; p = 0.08; KG66) and 110.85 ± 0.24 Ma (MSWD = 0.47; p = 0.98; KG67). Sample KG 64 yielded a mini-plateau age of 109.5 ± 0.7 (MSWD = 0.72; p = 0.69; ^{39}Ar = 60%). Pyroxene sample KG64 failed to yield a plateau.

$^{40}Ar/^{39}Ar$ ages of the four samples from the top flows (KG62, KG63, KG64, KG65) overlap with each other at 2σ but are slightly younger than the age of the bottommost sample (KG67). The age of sample KG66 is younger than the ages of the stratigraphically upper and lower flows (Fig. S6), which may indicate the timing of a late stage intrusive event.

Site 747, Central Kerguelen Plateau

Six analyses from five samples were conducted. One plagioclase sample yielded a $^{40}Ar/^{39}Ar$ plateau age of 92.8 ± 1.5 Ma (MSWD = 1.06; p = 0.38; KG14), while a groundmass sample yielded plateau age of 112.24 ± 0.97 Ma (MSWD = 1.10; p = 0.35; KG16) and could have been affected by secondary process as noted for other groundmass samples. The other plagioclase (KG16, KG20), pyroxene (KG15) and groundmass (KG16) samples failed to yield plateau ages.

Site 1138, Central Kerguelen Plateau

One plagioclase sample yielded a $^{40}Ar/^{39}Ar$ plateau age of 108.6 ± 2.2 Ma (MSWD = 0.33; p = 1.00; KG57).

Sites 1141 and 1142, Broken Ridge

One plagioclase sample yielded a $^{40}Ar/^{39}Ar$ plateau age of 99.13 ± 0.43 Ma (MSWD = 0.37; p = 0.99; KG 74). The groundmass samples yielded plateau ages of 91.84 ± 0.89 Ma (MSWD = 0.36; p = 0.99; KG77) and 95.7 ± 1.5 Ma (MSWD = 0.39; p = 0.99; KG78), which are both younger than the plagioclase age and might be caused by cryptic alteration.

RC27-10, RC27-8, Broken Ridge

Two plagioclase samples yielded consistent $^{40}Ar/^{39}Ar$ plateau ages of 97.7 ± 1.8 Ma (MSWD = 0.59; p = 0.93; KG50) and 97.5 ± 2.1 Ma (MSWD = 0.27; p = 1.00; KG51).

V. Mantle source components of the Kerguelen LIP in Figure 4

The isotopic signatures of the Kerguelen plume are best represented by the ca. 24 Ma Southeast Province lavas on the Kerguelen Archipelago (Fig. S7; Weis et al., 1993). Mixing modelling results show that the mantle source of the main portion of the Kerguelen LIP, including the Southern and Central Kerguelen Plateau, Elan Bank and Broken Ridge, can be explained by

mixing between the depleted MORB mantle (DMM) source and lithospheric mantle source (Olierook et al., 2017, 2019). The lithospheric mantle could be slivers of Gondwana lithosphere that was dispersed in the Indian Ocean during Gondwana breakup (cf. Frey et al., 2002). The younger (<93 Ma) and volumetrically minor portions of the Kerguelen LIP, including the Ninetyeast Ridge and Northern Kerguelen Plateau, were generated by a mixing source of the Kerguelen plume and DMM (Fig. S7; Olierook et al., 2017, 2019).

VI. Formation of the Ninetyeast Ridge and Northern Kerguelen Plateau

The Ninetyeast Ridge is a linear volcanic hotspot track formed by the Kerguelen plume since 83 Ma as the Indian plate drifted north (Duncan, 1991). After the formation of the Ninetyeast Ridge, the Kerguelen plume was located beneath the Kerguelen Archipelago (Fig. S8; Whittaker et al., 2013) and produced the Northern Kerguelen Plateau since ~34 Ma (Duncan, 2002). The Ninetyeast Ridge and Northern Kerguelen Plateau are volumetrically relatively minor portions of the Kerguelen LIP compared with the main construct of the LIP discussed in the main text.

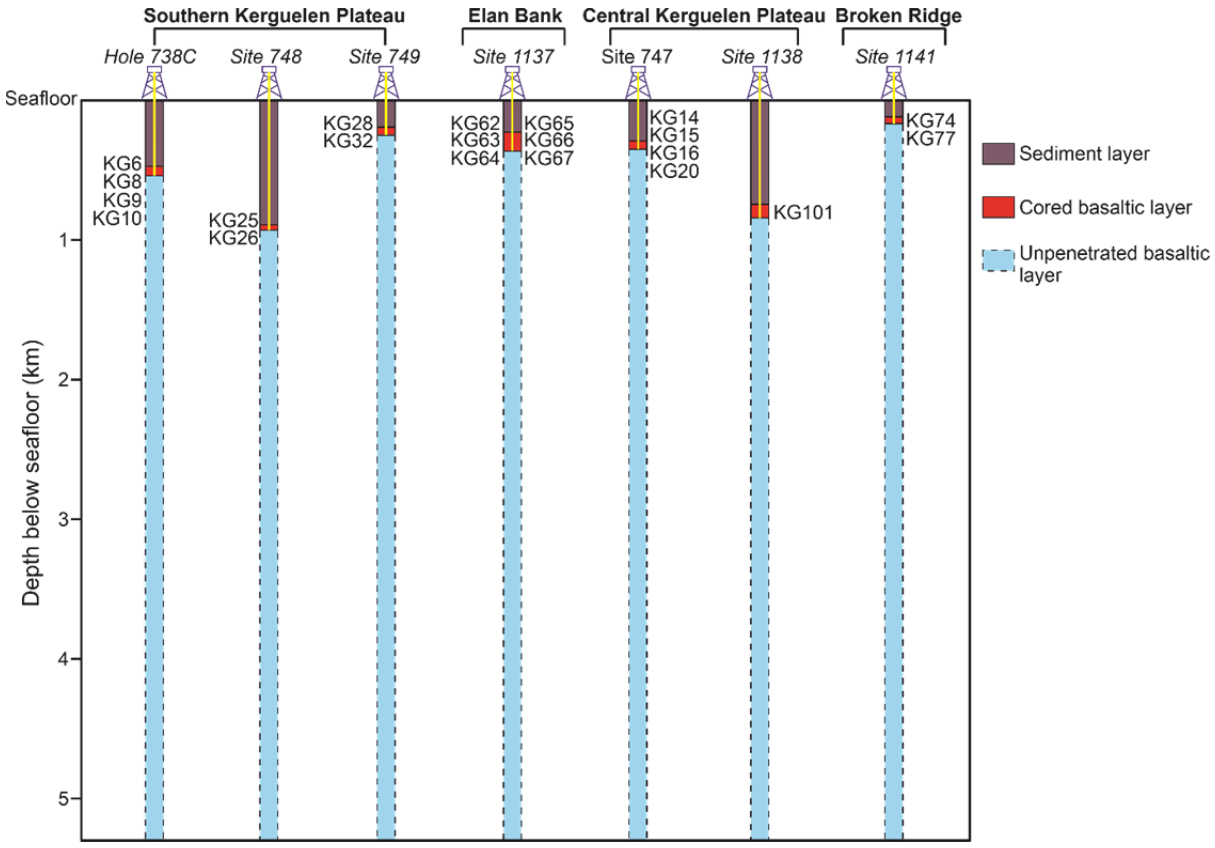

Figure S1. Schematic illustrations of stratigraphic locations of samples from the ODP drill holes. The average thickness of the basaltic layer is estimated by Borissova et al. (2003), Operto and Charvis (1996) and Charvis and Operto (1999) using wide-angle seismic data.

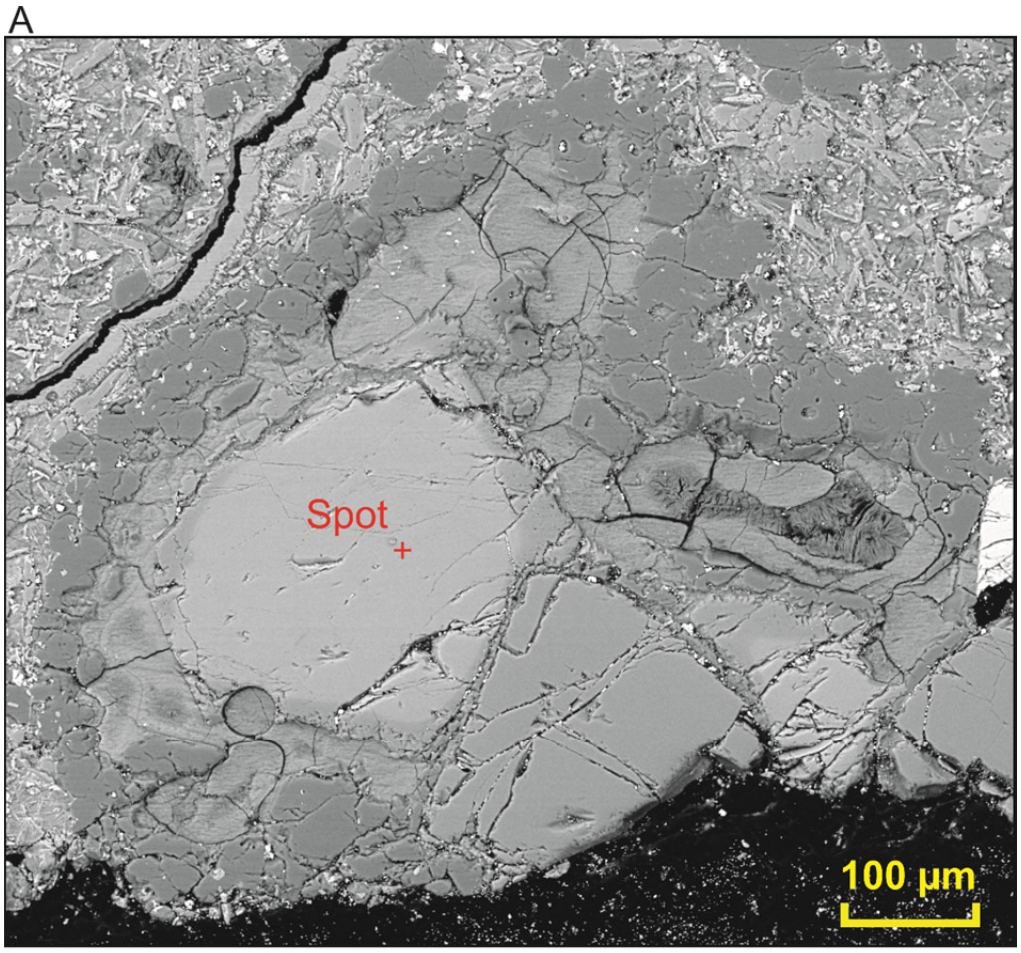

B

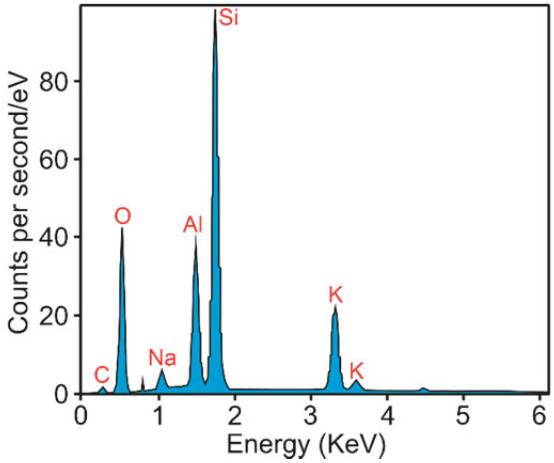

C

Element	Wt (%)	± 1σ
Oxygen (O)	46.18	0.19
Sodium (Na)	1.99	0.06
Aluminum (Al)	10.73	0.08
Silicon (Si)	30.50	0.13
Potassium (K)	10.60	0.08
Total	100.00	

Figure S2. Energy Dispersive X-ray (EDX) analysis of sanidine from sample KG 26. (A) Backscattered-Electron (BSE) image and analyzed spot. (B) EDX spectrum. (C) Quantify spectrum.

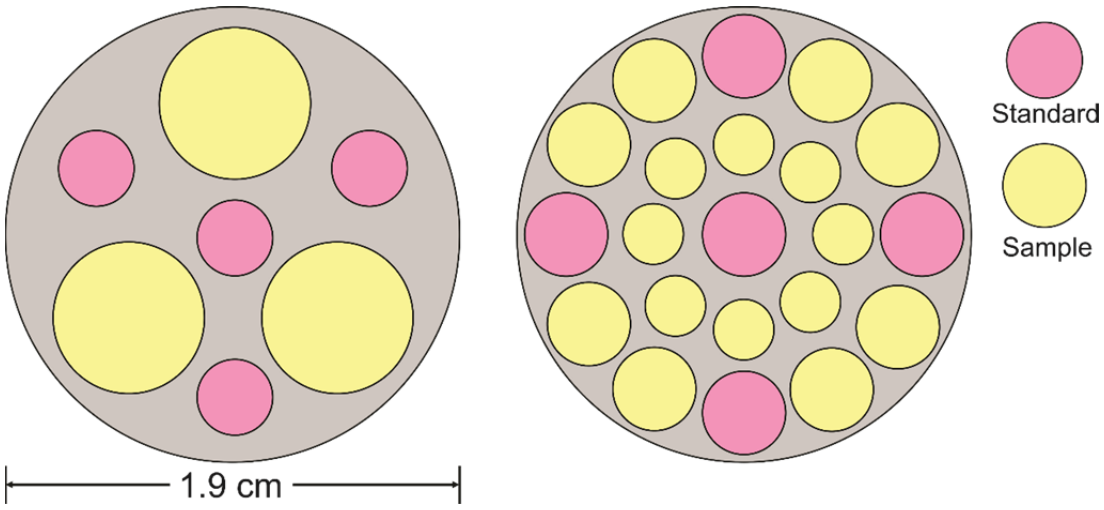

Figure S3. Geometry of the irradiation discs, showing relative locations of standards and samples during neutron irradiation.

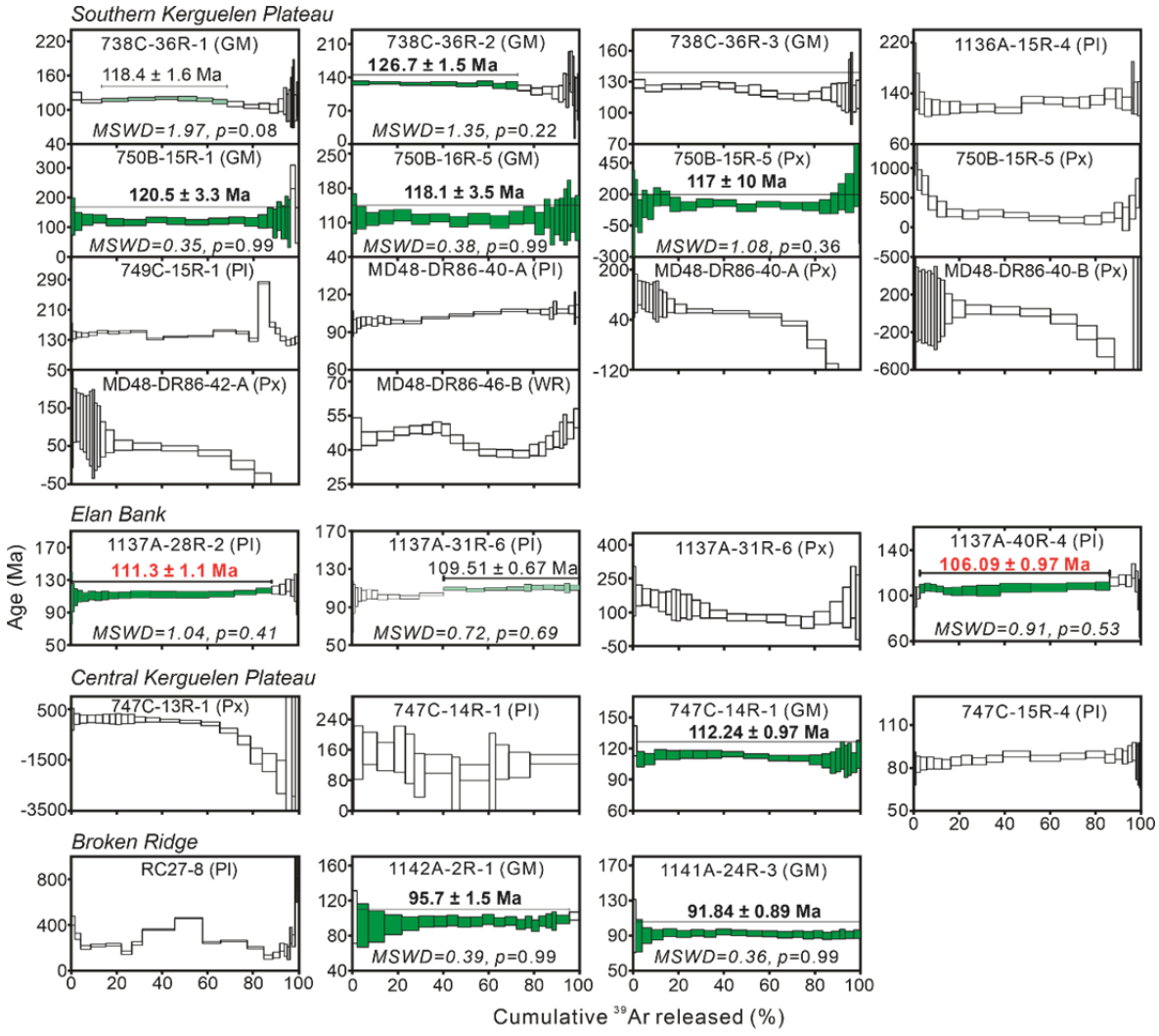

Figure S4. $^{40}Ar/^{39}Ar$ apparent age versus cumulative ^{39}Ar released. Plagioclase and sanidine $^{40}Ar/^{39}Ar$ plateaus from the Southern and Central Kerguelen Plateau, Elan Bank and Broken Ridge are shown in Figure 2. The age uncertainties include all sources of uncertainties and are quoted at 2σ. Pl—plagioclase, Px—pyroxene, GM—groundmass.

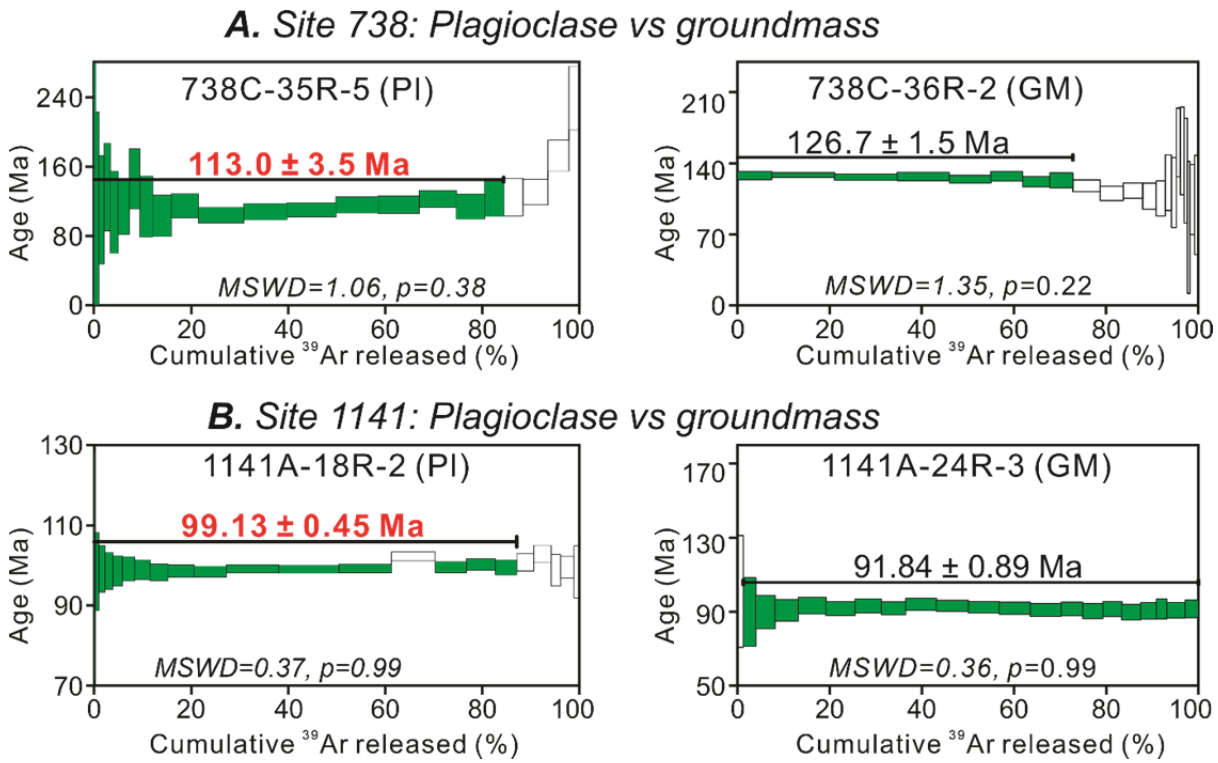

Figure S5. Comparison of $^{40}Ar/^{39}Ar$ plateau ages of plagioclase and groundmass separates from proximal samples in Sites 738 and 1141. The ages in red are the preferred ages derived from plagioclase, which clearly illustrate that inaccurate, yet well-defined plateau ages can be obtained using groundmass. Cf. also Hofmann et al. (2000), Jourdan et al. (2007), Renne et al. (2015) and Merle et al. (2019) for other comparative examples. The age uncertainties include all sources of uncertainties and are quoted at 2σ. Pl—plagioclase, GM—groundmass.

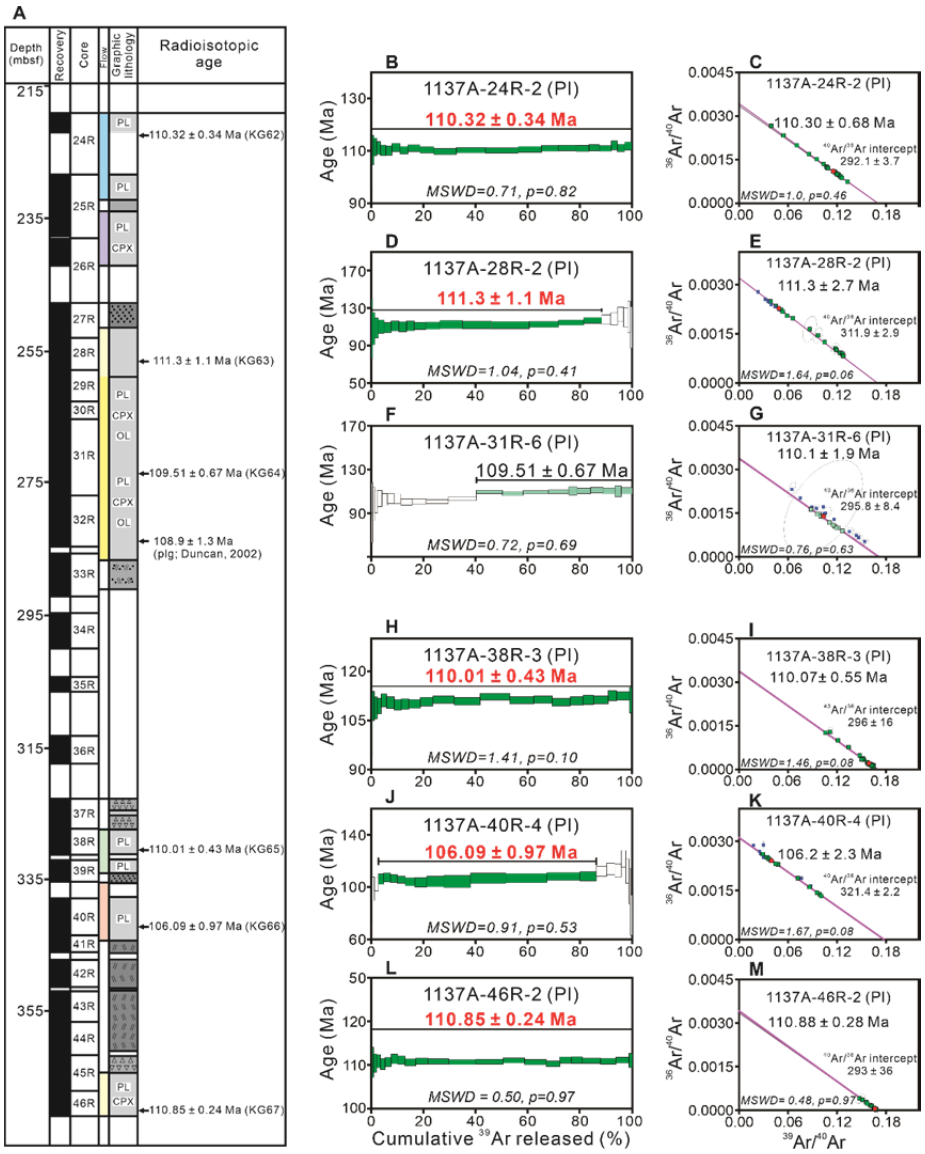

Figure S6. $^{40}Ar/^{39}Ar$ geochronology results of Site 1137, Elan Bank. (A) Stratigraphic section for Site 1137, after Shipboard Scientific Party (2000), and sample locations. (B, D, F, H, J, L) $^{40}Ar/^{39}Ar$ apparent age versus cumulative ^{39}Ar released. (C, E, G, I, K, M) $^{39}Ar/^{40}Ar$–$^{36}Ar/^{40}Ar$ isochron. The green and blue squares in the isochron plots indicate data that are used and not used in the calculation of isochron ages, respectively. The red circles indicate data for total fusion. Note that for sample 1137A-40R-4 (Pl) the $^{40}Ar/^{36}Ar$ intercept measured by the inverse isochron (321.4 ± 2.2) was used to calculate the plateau age. The ages in red are the preferred

ages. The age uncertainties include all sources of uncertainties and are quoted at 2σ. Pl—plagioclase.

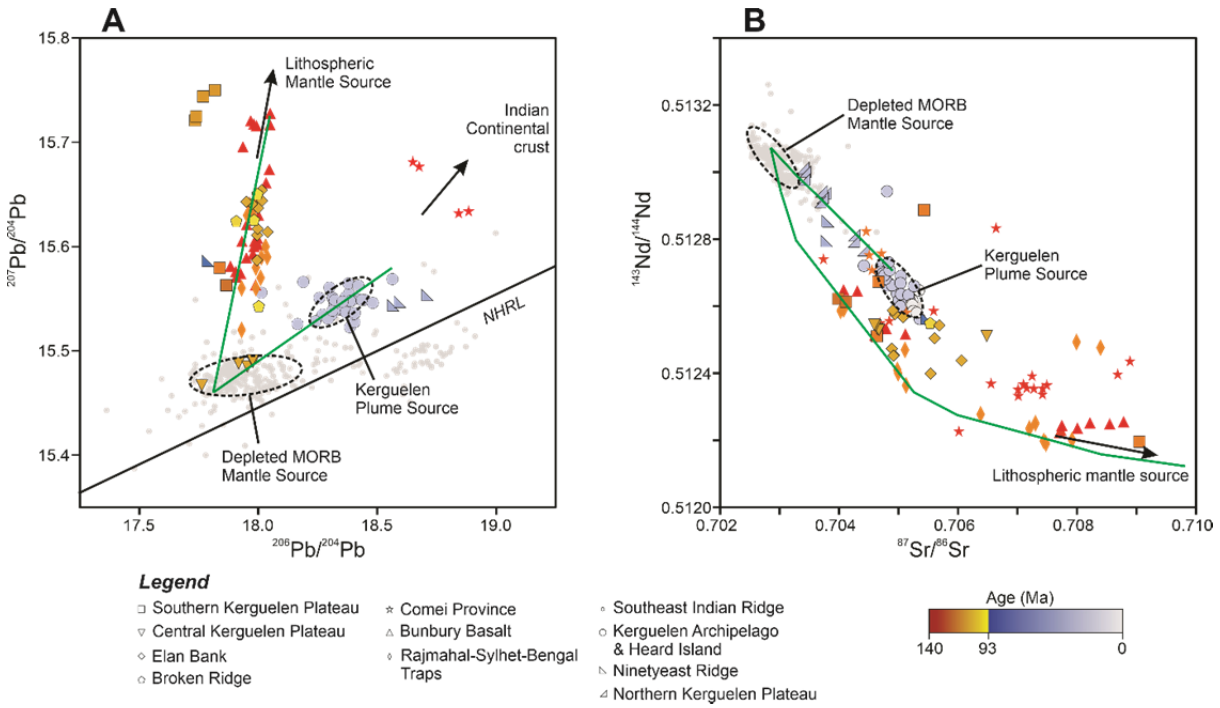

Figure S7. Sr-Nd-Pb isotope data of the Kerguelen LIP basalts, showing the mantle sources of the Kerguelen LIP. Isotope data and references are found in Table S5. The data were filtered for loss-on-ignition (LOI <2%), except for the depleted MORB mantle source, where there are few data with LOI <2%. The mixing curves (green solid lines) refer to Olierook et al. (2017).

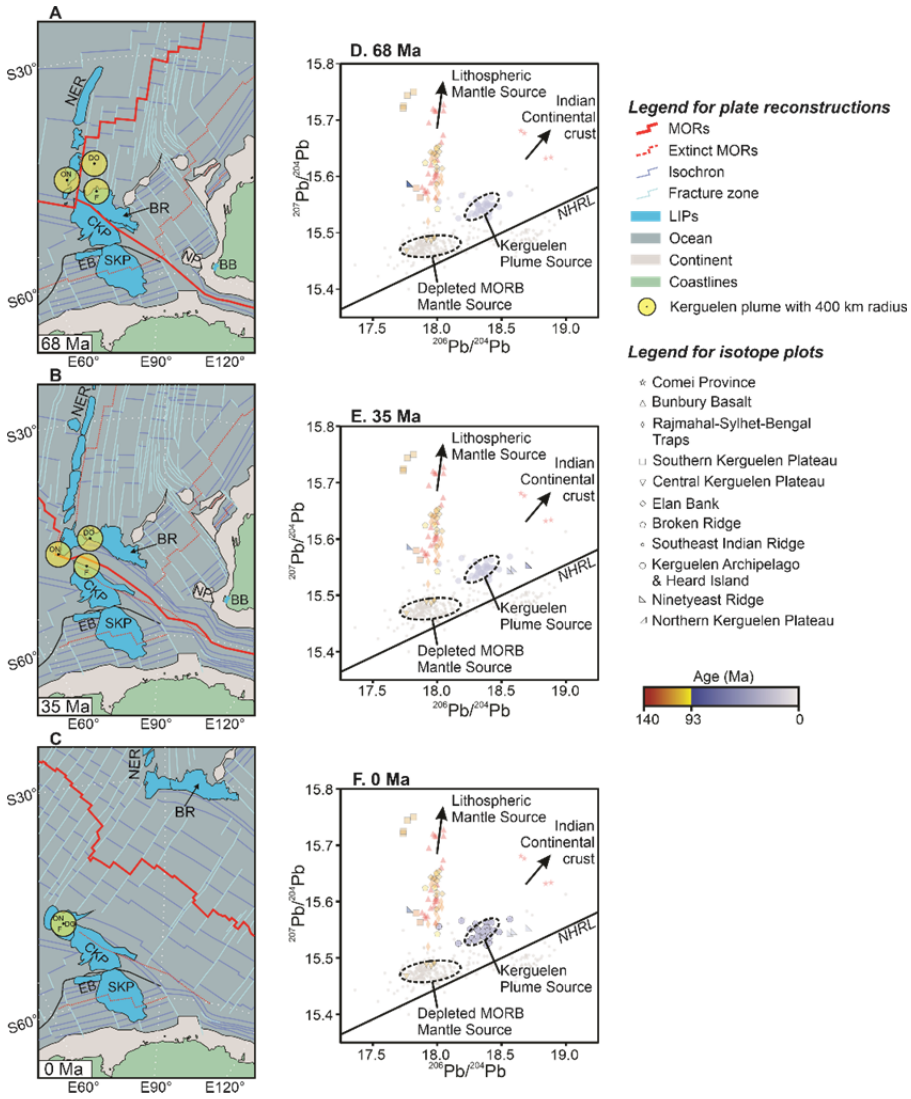

Figure S8. Formation of the Ninetyeast Ridge and Northern Kerguelen Plateau. (A–C), Plate reconstructions at 68 Ma, 35 Ma and 0 Ma (in a fixed Antarctica reference frame) after Gibbons et al. (2013) and Whittaker et al. (2013). Plume locations are DO—Doubrovine et al. (2012), F—Fixed plume (Müller et al., 1993), ON—O'Neill et al. (2005). (D–F) Isotope geochemical data of the basalts. Isotope geochemical data and references are found in Table S5. The data were filtered for loss-on-ignition (LOI <2%), except for the depleted MORB mantle source, where there is few data with LOI <2%. BR—Broken Ridge, CKP—Central Kerguelen Plateau, EB—

Elan Bank, NER—Ninetyeast Ridge, NHRL—Northern Hemisphere Reference Line (Hart, 1984), NKP—Northern Kerguelen Plateau, SKP—Southern Kerguelen Plateau.

Table S1. Compilation and evaluation of published $^{40}Ar/^{39}Ar$ data for basaltic samples from the main portion of the Kerguelen LIP

Sample Name	Method	Material	Age (Ma)	± 2σ	^{39}Ar in plateau (%)	MSWD	*p*	*n*	References	Why rejected?		
										Whole-rock	P < 0.05	^{39}Ar < 70%
Site 738, Southern Kerguelen Plateau												
119-738C-35R-2, 106-110	$^{40}Ar/^{39}Ar$ plateau	Whole rock	108.6	6	82	230	0.00	11	Coffin et al., 2002	×	×	
Site 747, Central Kerguelen Plateau												
120-747C-15R-2, 120-124	$^{40}Ar/^{39}Ar$ plateau	Whole rock	86.4	0.8	62	15.6	0.00	7	Coffin et al., 2002	×	×	×
	$^{40}Ar/^{39}Ar$ plateau	Whole rock	85.6	1	62	36.8	0.00	6	Coffin et al., 2002	×	×	×
Site 749, Southern Kerguelen Plateau												
120-749C-16R-5, 127-131	$^{40}Ar/^{39}Ar$ plateau	Plagioclase	114.2	3.4	93	10.6	0.00	7	Coffin et al., 2002		×	
Site 750, Southern Kerguelen Plateau												
120-750C-15R-5, 54-60	$^{40}Ar/^{39}Ar$ plateau	Whole rock	117.6	11.6	100	0.6	0.70	6	Whitechurch et al., 1992	×		
	$^{40}Ar/^{39}Ar$ plateau	**Plagioclase**	**112.6**	**1**	**100**	**1.44**	**0.17**	**9**				
120-750B-16R-2, 102-108	**$^{40}Ar/^{39}Ar$ plateau**	**Plagioclase**	**112.1**	**1.2**	**84**	**0.78**	**0.56**	**6**	**Coffin et al., 2002**			
	Weighted mean: 2 of 2 samples		**112.4**	**0.8**		**0.41**	**0.52**				**Good age**	
Site 1136, Southern Kerguelen Plateau												
183-1136A-16R-1, 84-89	**$^{40}Ar/^{39}Ar$ plateau**	**Plagioclase**	**118.99**	**2.11**	**98**	**1.11**	**0.35**	**7**	**Duncan, 2002**		**Good age**	
183-1136A-18R-2, 83-94	**$^{40}Ar/^{39}Ar$ plateau**	**Plagioclase**	**118.73**	**2.11**	**80**	**0.19**	**0.90**	**4**	**Duncan, 2002**		**Good age**	
183-1136A-19R-1, 63-68	$^{40}Ar/^{39}Ar$ plateau	Whole rock	115.23	0.96	57	1.04	0.39	6	Duncan, 2002	×		×
Site 1137, Elan Bank												
183-1137A-28R-4, 13-16	$^{40}Ar/^{39}Ar$ plateau	Whole rock	107.46	1.05	56	1.04	0.35	3	Duncan, 2002	×		×
183-1137A-32R-7, 52-59	**$^{40}Ar/^{39}Ar$ plateau**	**Plagioclase**	**107.07**	**1.27**	**94**	**1.79**	**0.10**	**7**	**Duncan, 2002**		**Good age**	
183-1137A-38R-4, 83-88	$^{40}Ar/^{39}Ar$ plateau	Whole rock	106.94	0.94	38	1.02	0.40	5	Duncan, 2002	×		×
183-1137A-40R-5, 67-74	$^{40}Ar/^{39}Ar$ plateau	Whole rock	107.53	1.04	58	1.06	0.37	5	Duncan, 2002	×		×
183-1137A-46R-2, 113-121	$^{40}Ar/^{39}Ar$ plateau	Whole rock	109.45	1.07	40	2.47	0.04	5	Duncan, 2002	×	×	×
Site 1138, Central Kerguelen Plateau												
183-1138A-80R-2, 126-134	$^{40}Ar/^{39}Ar$ plateau	Plagioclase	100.83	2.94	69	0.23	0.88	4	Duncan, 2002			×
183-1138A-80R-2, 126-134	$^{40}Ar/^{39}Ar$ plateau	Whole rock	100.24	1.09	88	2.22	0.08	4	Duncan, 2002	×		
183-1138A-84R-5, 88-93	$^{40}Ar/^{39}Ar$ plateau	Whole rock	100.51	1	77	1.82	0.12	5	Duncan, 2002	×		
Sites 1141 and 1142, Broken Ridge												
183-1141A-22R-3, 143-150	$^{40}Ar/^{39}Ar$ plateau	Whole rock	95.17	0.77	88	0.76	0.55	5	Duncan, 2002	×		
183-1142A-6R-1, 12-16	$^{40}Ar/^{39}Ar$ plateau	Whole rock	94.18	0.83	69	2.22	0.04	7	Duncan, 2002	×	×	×
183-1142A-9R-3, 91-94	$^{40}Ar/^{39}Ar$ plateau	Whole rock	94.88	0.9	71	2.11	0.04	8	Duncan, 2002	×	×	

Table S2. Published statistically reliable $^{40}Ar/^{39}Ar$ plateau and mini-plateau age data recalculated to the ^{40}K decay constants of Renne et al. (2011)

Sample Name	Method	Material	Original Age (Ma ± 2σ)	^{39}Ar in plateau (%)	MSWD	*p*	*n*	Standard	Original standard age (Ma)	Original Decay Constant ($\lambda_\varepsilon+\lambda_\beta$)	Recalculated standard age (Ma)*	Recalculated age (Ma ± 2σ) †	References
120-750B-16R-2, 102-108	$^{40}Ar/^{39}Ar$ plateau	Plagioclase	112.6 ± 1.0	100	1.44	0.17	9	USGS sanidine 85G003 (TCs)	28.34	5.543E-10	28.61	113.6 ± 1.0	Coffin et al., 2002
	$^{40}Ar/^{39}Ar$ plateau	Plagioclase	112.1 ± 1.2	84	0.78	0.56	6	USGS sanidine 85G003 (TCs)	28.34	5.543E-10	28.61	113.1 ± 1.2	
	Weighted mean:		112.4 ± 0.77		0.41	0.52						113.45 ± 0.83	
183-1136A-16R-1, 84-89	$^{40}Ar/^{39}Ar$ plateau	Plagioclase	119.0 ± 2.1	98	1.11	0.35	7	FCT-3 biotite	28.04	5.542E-10	28.54	121.0 ± 2.1	Duncan, 2002
183-1136A-18R-2, 83-94	$^{40}Ar/^{39}Ar$ plateau	Plagioclase	118.7 ± 2.1	80	0.19	0.90	4	FCT-3 biotite	28.04	5.542E-10	28.54	120.8 ± 2.1	Duncan, 2002
183-1137A-32R-7, 52-59	$^{40}Ar/^{39}Ar$ plateau	Plagioclase	107.1 ± 1.3	94	1.79	0.10	7	FCT-3 biotite	28.04	5.542E-10	28.54	108.9 ± 1.3	Duncan, 2002
183-1138A-80R-2, 126-134	$^{40}Ar/^{39}Ar$ plateau	Plagioclase	100.8 ± 2.9	69	0.23	0.88	4	FCT-3 biotite	28.04	5.542E-10	28.54	102.6 ± 3.0	Duncan, 2002

* Recalculated standard age compared to the age for the FCs standard (28.294 Ma) from Renne et al. (2011), using R[TCs/FCs] = 1.0112 (± 0.10%) and R[FCb/FCs] = 1.0086 (± 0.15%).

† Error includes all sources of uncertainties and was calculated using the method of Renne et al. (2010) and R-values uncertainties quoted above.

Table S3. New $^{40}Ar/^{39}Ar$ plateau and inverse isochron ages for basaltic samples from the Kerguelen Plateau and Broken Ridge

General characteristics				Plateau characteristics					Isochron characteristics					Preferred age[†]
Sample lab No.	**Drill core/Dredge site**	**Material**	**K/Ca**	**Plateau age (Ma ± 2σ)**	**^{39}Ar (%)**	**No. of steps**	**MSWD**	***p***	**Inv. isochron age (Ma ± 2σ)**	**n**	**$^{40}Ar/^{36}Ar$ intercept (± 2σ)**	**MSWD**	***p***	**(Ma ± $2\sigma_{int}$ [±$2\sigma_{ext}$])**
Site 738, Southern Kerguelen Plateau														
KG6	119-738C-35R-5, 107-122	Plagioclase	0.0156	**113.0 ± 3.5**	84	17 of 22	1.06	0.38	101 ± 12	17	430 ± 136	0.64	0.84	**113.0** ± 3.5 **[3.5]**
KG8	119-738C-36R-1, 62-78	Groundmass			No plateau						No isochron			-
KG9	119-738C-36R-2, 58-70	Groundmass	0.0573	126.7 ± 1.5	73	8 of 21	1.35	0.22	123.6 ± 3.7	8	334 ± 39	0.88	0.51	-
KG10	119-738C-36R-3, 9-24	Plagioclase	0.0198	109.5 ± 1.4	50	8 of 22	1.97	0.06	94 ± 16	8	627 ± 419	0.57	0.75	-
KG10	119-738C-36R-3, 9-24	Groundmass			No plateau						No isochron			-
Site 748, Southern Kerguelen Plateau														
KG25	120-748C-79R-6, 34-47	Sanidine	0.51	**96.49 ± 0.33**	98	16 of 17	0.45	0.96	96.0 ± 1.0	16	487 ± 559	0.4	0.98	**96.49** ± 0.33 **[0.35]**
KG26	120-748C-79R-7, 16-34	Sanidine	0.35	**96.79 ± 0.40**	100	17 of 17	0.38	0.99	96.90 ± 0.44	17	282 ± 33	0.34	0.99	**96.79** ± 0.40 **[0.42]**
Site 749, Southern Kerguelen Plateau														
KG28	120-749C-15R-1, 55-65	Plagioclase			No plateau						No isochron			-
KG32	120-749C-16R-6, 92-102	Plagioclase	0.0017	**122.2 ± 2.0** [‡]	100	23 of 23	0.28	1	122.2 ± 2.6	23	282.3 ± 6.2	0.31	1	**122.2** ± 2.0 **[2.0]**
Site 750, Southern Kerguelen Plateau														
KG52	120-750B-15R-1, 47-57	Groundmass	0.0131	120.5 ± 3.3	96	19 of 21	0.35	0.99	119.3 ± 5.1	19	300.9 ± 6.9	0.35	0.99	-
KG53	120-750B-15R-5, 30-40	Pyroxene	0.0001	117 ± 10	100	22 of 22	1.08	0.36	104 ± 17	22	302.9 ± 4.8	1.18	0.26	-
KG53R[*]	120-750B-15R-5, 30-40	Pyroxene			No plateau						No isochron			-
KG54	120-750B-16R-5, 14-24	Whole rock	0.0033	118.1 ± 3.5	100	21 of 21	0.38	0.99	117.4 ± 4.2	21	299.8 ± 3.9	0.38	0.99	-
1136, Southern Kerguelen Plateau														
KG57	183-1136A-15R-4, 12-24	Plagioclase			No plateau						No isochron			-
MD 48-40, Southern Kerguelen Plateau														
KG83	MD48-DR86-0040-A	Plagioclase			No plateau						No isochron			-
KG83R[*]	MD48-DR86-0040-A	Plagioclase	0.0522	**89.93 ± 0.96**	78	13 of 22	1.32	0.2	87.0 ± 4.9	13	381 ± 157	1.28	0.23	**89.93** ± 0.96 **[0.97]**
KG83	MD48-DR86-0040-A	Pyroxene			No plateau						No isochron			-
KG84	MD48-DR86-0040-B	Plagioclase	0.0132	**95.28 ± 0.42**	72	8 of 22	0.98	0.44	85 ± 13	8	412 ± 156	0.5	0.81	**95.28** ± 0.42 **[0.44]**
KG84	MD48-DR86-0040-B	Pyroxene			No plateau						No isochron			-
KG87	MD48-DR86-0042-A	Pyroxene			No plateau						No isochron			-
KG100	MD48-DR86-0046-B	Groundmass			No plateau						No isochron			-
Site 1137, Elan Bank														
KG62	183-1137A-24R-2, 26-36	Plagioclase	0.0191	**110.32 ± 0.31**[‡]	100	22 of 22	0.71	0.82	110.30 ± 0.68	22	292.1 ± 3.7	1	0.46	**110.32** ± 0.31 **[0.34]**
KG63	183-1137A-28R-2, 52-66	Plagioclase	0.0198	**111.3 ± 1.1**[‡]	88	16 of 22	1.04	0.41	111.3 ± 2.7	16	311.9 ± 2.9	1.64	0.06	**111.3** ± 1.1 **[1.1]**
KG64	183-1137A-31R-6, 33-43	Plagioclase	0.0201	109.51 ± 0.67	60	10 of 22	0.72	0.69	110.1 ± 1.9	10	295.8 ± 8.4	0.76	0.63	-
KG64	183-1137A-31R-6, 33-43	Pyroxene			No plateau						No isochron			-

KG65	183-1137A-38R-3, 48-58	Plagioclase	0.015	**110.01 ± 0.41**	100	22 of 22	1.41	0.1	110.07 ± 0.55	22	296 ± 16	1.46	0.08	**110.01** ± 0.41 **[0.43]**
KG 66	183-1137A-40R-4, 80-90	Plagioclase	0.0143	**106.09 ± 0.97**‡	83	12 of 22	0.91	0.53	106.2 ± 2.3	12	321.4 ± 2.2	1.67	0.08	**106.09** ± 0.97 **[0.99]**
KG 67	183-1137A-46R-2, 63-73	Plagioclase	0.0305	**110.85 ± 0.20**	100	22 of 22	0.47	0.98	110.88 ± 0.28	22	293 ± 36	0.48	0.97	**110.85** ± 0.20 **[0.24]**
Site 747, Central Kerguelen Plateau														
KG14	120-747C-13R-1, 32-47	Plagioclase	0.0092	**92.8 ± 1.5**	72	18 of 22	1.06	0.38	91.3 ± 2.3	18	315 ± 19	0.92	0.54	**92.8** ± 1.5 **[1.5]**
KG15	120-747C-13R-1, 82-96	Pyroxene			No plateau						No isochron			-
KG16	120-747C-14R-1, 5-15	Plagioclase			No plateau						No isochron			-
KG16	120-747C-14R-1, 5-15	Groundmass	0.0240	112.24 ± 0.97	98	20 of 21	1.10	0.35	112.2 ± 1.2	20	298.9 ± 3.8	1.15	0.30	-
KG20	120-747C-15R-4, 59-69	Plagioclase			No plateau						No isochron			-
Site 1138, Central Kerguelen Plateau														
KG101	183-1138A-80R-1, 11-21	Plagioclase	0.0029	**108.6 ± 2.2**	100	22 of 22	0.33	1	109.1 ± 2.2	22	293.7 ± 6.7	0.24	1	**108.6** ± 2.2 **[2.2]**
Sites 1141 and 1142, Broken Ridge														
KG74	183-1141A-18R-2,10-20	Plagioclase	0.016	**99.13 ± 0.43**	78	16 of 22	0.37	0.99	98.5 ± 1.5	16	330 ± 73	0.33	0.99	**99.13** ± 0.43 **[0.45]**
KG77	183-1141A-24R-3,8-20	Groundmass	0.040	91.84 ± 0.89	99	20 of 21	0.36	0.99	92.6 ± 2.7	20	297. 6 ± 3.6	0.37	0.99	-
KG78	183-1142A-2R-1,86-98	Groundmass	0.0259	95.7 ± 1.5	93	19 of 21	0.39	0.99	97.2 ± 3.5	19	296.6 ± 4.1	0.36	0.99	-
RC 27-10, Broken Ridge														
KG50	RC 27-10-A4	Plagioclase	0.002	**97.7 ± 1.8**	100	22 of 22	0.59	0.93	98.4 ± 3.4	22	296.3 ± 8.8	0.61	0.91	**97.7** ± 1.8 **[1.8]**
KG51	RC 27-10-A5	Plagioclase	0.0022	**97.5 ± 2.1**	100	22 of 22	0.27	1	98.3 ± 2.3	22	294.9 ± 4.8	0.17	1	**97.5** ± 2.1 **[2.1]**
RC27-8, Broken Ridge														
KG48	RC27-8	Plagioclase			No plateau						No isochron			-
RC17-6, Northern Kerguelen Plateau														
KG38	RC17-6-A	Plagioclase	0.014	**26.91 ± 0.28**	100	22 of 22	0.71	0.83	26.89 ± 0.34	22	299.4 ± 7.0	0.74	0.79	**26.91** ± 0.28 **[0.31]**
KG38	RC17-6-A	Pyroxene	0.0002	27 ± 10	100	23 of 23	0.52	0.97	22.0 ± 9.8	23	305 ± 11	0.49	0.98	-
KG40	RC17-6-C	Pyroxene	0.0015	**26.9 ± 4.0**	78	15 of 23	0.33	0.99	26 ± 11	15	299.1 ± 6.0	0.35	0.98	**26.9** ± 4.0 **[4.0]**
KG41	RC17-6-D	Groundmass	0.039	23.08 ± 0.43	100	21 of 21	1.09	0.35	23.4 ± 1.1	21	297.9 ± 2.3	1.14	0.30	-
KG42	RC17-6-E	Groundmass			No plateau						No isochron			-
ELT 46, Northern Kerguelen Plateau														
KG43	ELT 46-5042	Glass	0.233	**0.344 ± 0.049**‡	94	17 of 21	1.38	0.14	0.345 ± 0.066	17	296.2 ± 1.3	0.63	0.85	**0.344** ± 0.049 **[0.049]**
KG43	ELT 46-5042	Pyroxene	0.0032	7.8 ± 3.8	88	18 of 23	0.92	0.55	10.3 ± 3.7	18	295 ± 19	0.99	0.46	-

*Re-analysis.

†Errors shown as ± x [y] for internal error (including analytical and J-value errors; x), and external error (including all sources of error; y).

‡ Measured $^{40}Ar/^{36}Ar$ intercept ratio was used to calculate the plateau age.

References

Baksi, A. K., 2007, A quantitative tool for evaluating alteration in undisturbed rocks and minerals— I: water, chemical weathering and atmospheric argon, *in* Foulger, G. R., and Jurdy, D.M., ed., Plates, plumes, and planetary processes: Geological Society of America Special Papers, v. 430, p. 285–303, https://doi.org/10.1130/2007.2430(15).

Borissova, I., Coffin, M. F., Charvis, P., and Operto, S., 2003, Structure and development of a microcontinent: Elan Bank in the southern Indian Ocean: Geochemistry, Geophysics, Geosystems, v. 4, https://doi.org/10.1029/2003GC000535.

Charvis, P., and Operto, S., 1999, Structure of the Cretaceous Kerguelen Volcanic Province (southern Indian Ocean) from wide-angle seismic data.: Journal of Geodynamics, v. 28, p. 51-71, https://doi.org/10.1016/S0264-3707(98)00029-5.

Coffin, M. F., Pringle, M. S., Duncan, R. A., Gladczenko, T. P., Storey, M., Müller, R. D., and Gahagan, L. A., 2002, Kerguelen hotspot magma output since 130 Ma: Journal of Petrology, v. 43, p. 1121-1139, https://doi.org/10.1093/petrology/43.7.1121.

Doubrovine, P. V., Steinberger, B., and Torsvik, T. H., 2012, Absolute plate motions in a reference frame defined by moving hot spots in the Pacific, Atlantic, and Indian oceans: Journal of Geophysical Research: Solid Earth, v. 117, https://doi.org/10.1029/2011JB009072.

Duncan, R. A., 1991, Age distribution of volcanism along aseismic ridges in the eastern Indian Ocean, Proceedings of the Ocean Drilling Program, Scientific Results, v. 121: College Station, TX, p. 507-517.

Duncan, R. A., 2002, A time frame for construction of the Kerguelen Plateau and Broken Ridge: Journal of Petrology, v. 43, p. 1109-1119, https://doi.org/10.1093/petrology/43.7.1109.

Frey, F. A., Weis, D., Borisova, A. Y., and Xu, G., 2002, Involvement of continental crust in the formation of the Cretaceous Kerguelen Plateau: New perspectives from ODP Leg 120 sites: Journal of Petrology, v. 43, p. 1207-1239, https://doi.org/10.1093/petrology/43.7.1207.

Gibbons, A. D., Whittaker, J. M., and Müller, R. D., 2013, The breakup of East Gondwana: Assimilating constraints from Cretaceous ocean basins around India into a best-fit tectonic model: Journal of Geophysical Research: Solid Earth, v. 118, p. 808-822, https://doi.org/10.1002/jgrb.50079.

Hart, S. R., 1984, A large-scale isotope anomaly in the Southern Hemisphere mantle: Nature, v. 309, p. 753-757, https://doi.org/10.1038/309753a0.

Hofmann, C., Feraud, G., and Courtillot, V., 2000, $^{40}Ar/^{39}Ar$ dating of mineral separates and whole rocks from the Western Ghats lava pile: further constraints on duration and age of the Deccan traps: Earth and Planetary Science Letters, v. 180, p. 13-27, https://doi.org/10.1016/S0012-821x(00)00159-X.

Jourdan, F., Feraud, G., Bertrand, H., Watkeys, M., and Renne, P. R., 2007, Distinct brief major events in the Karoo large igneous province clarified by new $^{40}Ar/^{39}Ar$ ages on the Lesotho basalts: Lithos, v. 98, p. 195-209, https://doi.org/10.1016/j.lithos.2007.03.002.

Jourdan, F., and Renne, P. R., 2007, Age calibration of the Fish Canyon sanidine $^{40}Ar/^{39}Ar$ dating standard using primary K-Ar standards: Geochimica Et Cosmochimica Acta, v. 71, p. 387-402, https://doi.org/10.1016/j.gca.2006.09.002.

Koppers, A. A. P., 2002, ArArCALC—software for $^{40}Ar/^{39}Ar$ age calculations: Computers & Geosciences, v. 28, p. 605-619, https://doi.org/10.1016/S0098-3004(01)00095-4.

Lee, J. Y., Marti, K., Severinghaus, J. P., Kawamura, K., Yoo, H. S., Lee, J. B., and Kim, J. S., 2006, A redetermination of the isotopic abundances of atmospheric Ar:

Geochimica Et Cosmochimica Acta, v. 70, p. 4507-4512, https://doi.org/10.1016/j.gca.2006.06.1563.

Merle, R. E., Jourdan, F., Chiaradia, M., Olierook, H. K. H., and Manatschal, G., 2019, Origin of widespread Cretaceous alkaline magmatism in the Central Atlantic: A single melting anomaly?: Lithos, v. 342, p. 480-498, https://doi.org/10.1016/j.lithos.2019.06.002.

Müller, R. D., Royer, J. Y., and Lawver, L. A., 1993, Revised plate motions relative to the hotspots from combined Atlantic and Indian Ocean hotspot tracks: Geology, v. 21, p. 275-278, https://doi.org/10.1130/0091-7613(1993)021<0275:RPMRTT>2.3.CO;2.

Olierook, H. K. H., Jiang, Q., Jourdan, F., and Chiaradia, M., 2019a, Greater Kerguelen large igneous province reveals no role for Kerguelen mantle plume in the continental breakup of eastern Gondwana: Earth and Planetary Science Letters, v. 511, p. 244-255, https://doi.org/10.1016/j.epsl.2019.01.037.

Olierook, H. K. H., Merle, R. E., and Jourdan, F., 2017, Toward a Greater Kerguelen large igneous province: Evolving mantle source contributions in and around the Indian Ocean: Lithos, v. 282, p. 163-172, https://doi.org/10.1016/j.lithos.2017.03.007.

O'Neill, C., Müller, D., and Steinberger, B., 2005, On the uncertainties in hot spot reconstructions and the significance of moving hot spot reference frames: Geochemistry, Geophysics, Geosystems, v. 6, https://doi.org/10.1029/2004GC000784.

Oostingh, K. F., Jourdan, F., Matchan, E. L., and Phillips, D., 2017, $^{40}Ar/^{39}Ar$ geochronology reveals rapid change from plume-assisted to stress-dependent volcanism in the Newer Volcanic Province, SE Australia: Geochemistry, Geophysics, Geosystems, v. 18, p. 1065-1089, https://doi.org/10.1002/2016GC006601.

Operto, S., and Charvis, P., 1996, Deep structure of the southern Kerguelen Plateau (southern Indian Ocean) from ocean bottom seismometer wide-angle seismic data: Journal of

Geophysical Research: Solid Earth, v. 101, p. 25077-25103, https://doi.org/10.1029/96jb01758.

Phillips, D., and Matchan, E. L., 2013, Ultra-high precision $^{40}Ar/^{39}Ar$ ages for Fish Canyon Tuff and Alder Creek Rhyolite sanidine: New dating standards required?: Geochimica et Cosmochimica Acta, v. 121, p. 229-239, https://doi.org/10.1016/j.gca.2013.07.003.

Renne, P. R., Balco, G., Ludwig, K. R., Mundil, R., and Min, K., 2011, Response to the comment by W.H. Schwarz et al. on "Joint determination of ^{40}K decay constants and $^{40}Ar^*/^{40}K$ for the Fish Canyon sanidine standard, and improved accuracy for $^{40}Ar/^{39}Ar$ geochronology" by P.R. Renne et al. (2010): Geochimica Et Cosmochimica Acta, v. 75, p. 5097-5100, https://doi.org/10.1016/j.gca.2011.06.021.

Renne, P. R., Deino, A. L., Hilgen, F. J., Kuiper, K. F., Mark, D. F., Mitchell, W. S., Morgan, L. E., Mundil, R., and Smit, J., 2013, Time Scales of Critical Events Around the Cretaceous-Paleogene Boundary: Science, v. 339, p. 684-687, https://doi.org/10.1126/science.1230492.

Renne, P. R., Mundil, R., Balco, G., Min, K., and Ludwig, K. R., 2010, Joint determination of ^{40}K decay constants and $^{40}Ar^*/^{40}K$ for the Fish Canyon sanidine standard, and improved accuracy for $^{40}Ar/^{39}Ar$ geochronology: Geochimica et Cosmochimica Acta, v. 74, p. 5349-5367, https://doi.org/10.1016/j.gca.2010.06.017.

Renne, P. R., Sprain, C. J., Richards, M. A., Self, S., Vanderkluysen, L., and Pande, K., 2015, State shift in Deccan volcanism at the Cretaceous-Paleogene boundary, possibly induced by impact: Science, v. 350, p. 76-78, https://doi.org/10.1126/science.aac7549.

Renne, P. R., Swisher, C. C., Deino, A. L., Karner, D. B., Owens, T. L., and DePaolo, D. J., 1998, Intercalibration of standards, absolute ages and uncertainties in $^{40}Ar/^{39}Ar$ dating: Chemical Geology, v. 145, p. 117-152, https://doi.org/10.1016/S0009-2541(97)00159-9.

Schaen, A. J., Jicha, B. R., Hodges, K. V., Vermeesch, P., Stelten, M. E., Mercer, C. M., Phillips, D., Rivera, T. A., Jourdan, F., Matchan, E. L., Hemming, S. R., Morgan, L. E., Kelley, S. P., Cassata, W. S., Heizler, M. T., Vasconcelos, P. M., Benowitz, J. A., Koppers, A. A. P., Mark, D. F., Niespolo, E. M., Sprain, C. J., Hames, W. E., Kuiper, K. F., Turrin, B. D., Renne, P. R., Ross, J., Nomade, S., Guillou, H., Webb, L. E., Cohen, B. A., Calvert, A. T., Joyce, N., Ganerød, M., Wijbrans, J., Ishizuka, O., He, H., Ramirez, A., Pfänder, J. A., Lopez-Martínez, M., Qiu, H., and Singer, B. S., 2020, Interpreting and reporting $^{40}Ar/^{39}Ar$ geochronologic data: Geological Society of America Bulletin, https://doi.org/10.1130/B35560.1 (in press).

Shipboard Scientific Party, 1989, Site 748. *in* Schlich, R., Wise Jr, S. W., et al., Proceedings of the Ocean Drilling Program, Initial Reports, 120: College Station, Texas, p. 157–235, https://doi.org/10.2973/odp.proc.ir.120.110.1989.

Shipboard Scientific Party, 2000, Site 1137, *in* Coffin, M. F., Frey, F. A., Wallace, P. J., et al., Proceedings of the Ocean Drilling Program, Initial Reports Volume 183: College Station, Texas, p. 1–202, https://doi.org/10.2973/odp.proc.ir.183.105.2000.

Steiger, R. H., and Jäger, E., 1977, Subcommission on geochronology: convention on the use of decay constants in geo-and cosmochronology: Earth and Planetary Science Letters, v. 36, p. 359-362, https://doi.org/10.1016/0012-821X(77)90060-7.

Ware, B., and Jourdan, F., 2018, $^{40}Ar/^{39}Ar$ geochronology of terrestrial pyroxene: Geochimica Et Cosmochimica Acta, v. 230, p. 112-136, https://doi.org/10.1016/j.gca.2018.04.002.

Weis, D., Frey, F., Leyrit, H., and Gautier, I., 1993, Kerguelen Archipelago revisited: geochemical and isotopic study of the Southeast Province lavas: Earth and Planetary Science Letters, v. 118, p. 101-119, https://doi.org/10.1016/0012-821X(93)90162-3.

Whittaker, J. M., Williams, S. E., and Müller, R. D., 2013, Revised tectonic evolution of the Eastern Indian Ocean: Geochemistry, Geophysics, Geosystems, v. 14, p. 1891-1909, https://doi.org/10.1002/ggge.20120.